



OPEN

## Circular dichroism in multiphoton ionization of resonantly excited helium ions near channel closing

René Wagner<sup>1,2</sup>, Markus Ilchen<sup>1,2,3,4</sup>, Nicolas Douguet<sup>5</sup>, Philipp Schmidt<sup>1</sup>, Niclas Wieland<sup>2</sup>, Carlo Callegari<sup>6</sup>, Zachary Delk<sup>7</sup>, Alexander Demidovich<sup>6</sup>, Giovanni De Ninno<sup>6</sup>, Michele Di Fraia<sup>6</sup>, Jiri Hofbrucker<sup>8</sup>, Michele Manfredda<sup>6</sup>, Valerija Music<sup>1,3,4</sup>, Oksana Plekan<sup>6</sup>, Kevin C. Prince<sup>6</sup>, Daniel E. Rivas<sup>1</sup>, Marco Zangrando<sup>6,9</sup>, Alexei N. Grum-Grzhimailo<sup>10</sup>, Klaus Bartschat<sup>11</sup> & Michael Meyer<sup>1</sup>✉

The circular dichroism (CD) of photoelectrons generated by near-infrared (NIR) laser pulses using multiphoton ionization of excited  $\text{He}^+$  ions in the  $3p(m=+1)$  state is investigated. The ions were prepared by circularly polarized extreme ultraviolet (XUV) pulses. For circularly polarized NIR pulses co- and counter-rotating relative to the polarization of the XUV pulse, a complex variation of the CD is observed as a result of intensity- and polarization-dependent Freeman resonances, with and without additional dichroic AC-Stark shifts. The experimental results are compared with numerical solutions of the time-dependent Schrödinger equation to identify and interpret the pronounced variation of the experimentally observed CD.

Photoionization with circularly polarized light can provide unique information about the dynamics and fundamentals of light-matter interaction. In particular, the circular dichroism (CD) in photoemission experiments, i.e., the difference in the ionization signal between configurations using opposite light helicities, were successfully explored at synchrotron radiation facilities<sup>1,2</sup> and with intense optical lasers<sup>3–5</sup>. Various phenomena can be examined, such as isotope effects in atomic photoionization, which reveal the coupling between electronic and nuclear angular momenta<sup>6</sup>, information on the chirality of molecular systems, e.g., via measurements of the photoelectron circular dichroism<sup>7–11</sup> and its relevance for ionization and dissociation processes<sup>12</sup>, as well as the magnetic properties and magnetization dynamics of various materials<sup>13</sup>. In studies dedicated to tunnel ionization via strong fields<sup>4,14</sup>, it was predicted and demonstrated that ionization is favored for electrons that are initially orbiting against the laser field. Whether this is a general phenomenon or only evident under specific conditions is still under debate. In pump-probe experiments, ionization with counter-rotating pulses could thus be stronger than ionization with co-rotating pulses.

Recent experiments dedicated to CD studies in the nonlinear regime<sup>15–17</sup> have been made possible by short-wavelength free-electron lasers (FELs). One commonly used tool is the so-called “sideband method”, where the photoelectrons are dressed by a synchronized optical or infrared (IR) laser field. This results in additional spectral contributions to the photoelectron line, which are separated by the energy of the optical laser photons. The variation of the relative intensity of the sidebands for different combinations of circularly polarized FEL and optical pulses was used to determine the polarization state of X-ray or XUV radiation<sup>15,18</sup> and the relative intensity of partial-wave contributions<sup>19</sup>.

Even more information about the complex interactions in the electronic cloud is accessible via the study of resonances and transient states<sup>20</sup>. The precise characterization of their energy position, absorption strength, and spectral profile provides rich information about both the interactions in the electronic subshells of the target atom and the coupling to the ionization continuum. In particular, high-intensity laser fields can be used to steer

<sup>1</sup>European X-Ray Free-Electron Laser Facility, 22869 Schenefeld, Germany. <sup>2</sup>Department of Physics, Universität Hamburg, 22607 Hamburg, Germany. <sup>3</sup>Deutsches Elektronen-Synchrotron DESY, Notkestr. 85, 22607 Hamburg, Germany. <sup>4</sup>Institut für Physik und CINSaT, Universität Kassel, 34132 Kassel, Germany. <sup>5</sup>Department of Physics, University of Central Florida, Orlando, FL 32816, USA. <sup>6</sup>Elettra-Sincrotrone Trieste S.C.p.A., 34149 Basovizza, Trieste, Italy. <sup>7</sup>Department of Physics, Kennesaw State University, Marietta, GA 30060, USA. <sup>8</sup>Deutsches Elektronen-Synchrotron DESY, Notkestr. 85, 22607 Hamburg, Germany. <sup>9</sup>CNR Istituto Officina dei Materiali, Laboratorio TASC, 34149 Basovizza, Trieste, Italy. <sup>10</sup>Skobeltsyn Institute of Nuclear Physics, Lomonosov Moscow State University, Moscow 119991, Russia. <sup>11</sup>Department of Physics and Astronomy, Drake University, Des Moines, IA 50311, USA. ✉email: michael.meyer@xfel.eu

specific and also transient states into resonance, a phenomenon known as Freeman resonances<sup>21,22</sup>. In this case the photoionization dynamics are strongly affected by the symmetry of the intermediate resonant state.

In order to study the fundamental principles in detail experimentally and theoretically, small systems with few or preferably only one electron are desirable. In this regard, single-electron helium ions are ideal targets, since the alternative, the hydrogen atom, is particularly challenging to investigate experimentally. Hydrogen-like oriented helium ions created through sequential ionization and absorption by a circularly polarized FEL pulse thus offer a vital alternative for detailed investigations of dichroic phenomena<sup>17</sup> and the respective role of intermediate resonances. Studies of the latter have been elusive in practice until very recently, in particular regarding their role in the photoionization of transient and ionic systems.

In the present work, laser-based multiphoton ionization (MPI) via a  $\text{He}^+3p$  ( $m=+1$ ) oriented state created by intense, circularly polarized, extreme ultraviolet (XUV) radiation from the XUV-FEL FERMI<sup>23</sup> is used to study the polarization- and intensity-dependent yields, kinetic energies, and dichroic properties of the resulting photoelectrons (see Fig. 1). In particular, we investigate the dependence of the CD over a range of near-infrared (NIR) laser intensities ranging from  $10^{12} \text{ W/cm}^2$  to  $10^{13} \text{ W/cm}^2$  with a central wavelength of 784 nm. The CD is defined as

$$\text{CD} \equiv \frac{P_+ - P_-}{P_+ + P_-}. \quad (1)$$

Here  $P_+$  and  $P_-$  are the probabilities for ionization by circularly polarized pulses with the same (+) or opposite (-) helicity, respectively.

In our earlier work<sup>17</sup>, using temporally overlapping XUV and NIR pulses, the observed intensity dependence of the CD was explained mainly by the strong, NIR-induced AC-Stark shift of the  $3p$  resonance in  $\text{He}^+$ , which shifted the resonance position out of the spectral width of the XUV pulse. The resulting intensity- and polarization-dependent variation of the  $\text{He}^+3p$  population gave the largest contribution to the observed changes in the CD of the multi-photon ionization from the  $\text{He}^+3p$  state by the NIR pulse. In the present study, we eliminate this influence on the population of the  $\text{He}^+$  ions in the  $3p$  ( $m=+1$ ) oriented state by delaying the optical laser pulse by 500 fs in time, i.e., we first create the oriented ions and subsequently ionize them with the optical laser after the FEL pulse has fully passed.

The chosen intensity range includes not only multi-photon interactions but also over-the-barrier effects and can thus yield information about characteristic regimes of the Keldysh parameter in order to draw a comprehensive picture of circular dichroism in a wide range of field strengths. Specifically, for an ionization potential of  $\approx 6 \text{ eV}$ , the Keldysh parameter in the present study ranges from  $\approx 2.3$  for  $10^{13} \text{ W/cm}^2$  to  $\approx 10$  for  $5 \times 10^{11} \text{ W/cm}^2$ , respectively. Since for higher NIR intensities the binding energy of electrons is being shifted to

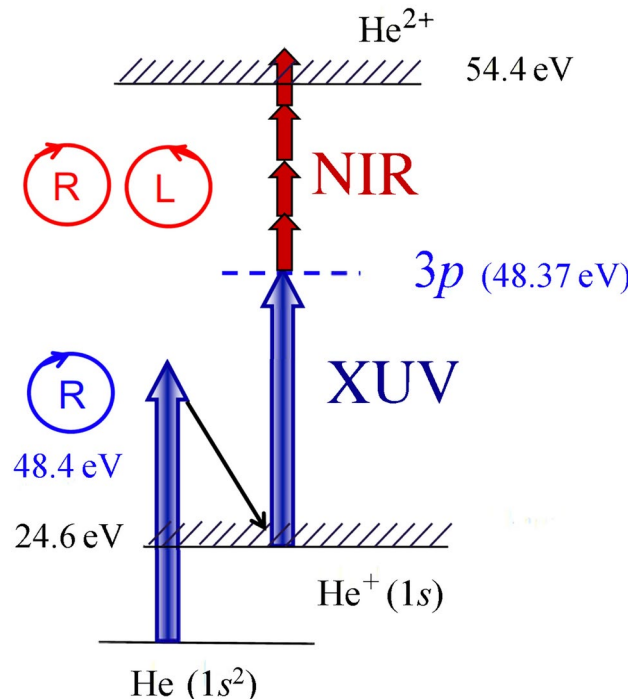


**Fig. 1.** Schematic representation of the ionization and excitation processes. Right-handed circularly polarized XUV radiation ionizes the helium atom and subsequently excites the  $\text{He}^+(3p, m=+1)$  resonance. Intense left- or right-handed circularly polarized NIR pulses further ionize the excited ions via a multiphoton process. The energies of the  $3p$  state and the ionization threshold of  $\text{He}^{2+}$  are given relative to the  $\text{He}^+(1s)$  ground state..

values higher than four times the NIR photon energy, the electrons require an additional NIR photon to enter the continuum. In the corresponding intensity range, we reveal not only the intensity-dependent role of Rydberg resonances on the dichroic yields of multiphoton ionization (MPI) and above-threshold ionization (ATI), but also analyze the previously debated sign change of the dichroism that was hitherto only predicted by theory for an AC-Stark-shift-influenced system<sup>17</sup>. Our observations thus contribute to shedding light on fundamental properties of dichroic light-matter interactions and the claimed predominant role of counter-rotating fields in the high-intensity regime<sup>4,14,24</sup>.

This paper is organized as follows. “**Methods**” summarizes the experimental (“**Experiment**”) and theoretical (“**Theory**”) methods employed in the present work. This is followed by a presentation and discussion of our results in “**Results and Discussion**”. Our conclusions and an outlook are given in in “**Conclusions and Outlook**”.

## Methods

### Experiment

The experiments were performed at the Low-Density Matter (LDM) end-station<sup>25</sup> of the seeded free-electron laser FERMI<sup>26</sup>. The circularly polarized XUV pulses from the FEL-1 laser were tuned to the  $3p$  resonance of the helium ion at 48.37 eV (25.63 nm) square envelope of the vector potential square envelope of the vector potential<sup>27</sup> (under field-free conditions), which was excited by sequential two-photon absorption within the FEL pulse duration of  $75 \text{ fs} \pm 25 \text{ fs}$  (FWHM).

With pulse energies up to  $150 \mu\text{J}$  and a focus size of  $10\text{-}20 \mu\text{m}$  (FWHM), the peak intensity of the XUV radiation was about  $10^{15} \text{ W/cm}^2$ . The repetition rate of the FEL pulses was 50 Hz, and the degree of circular polarization was  $95\% \pm 5\%$ <sup>15</sup>.

The circularly polarized NIR laser had a mean photon energy of 1.58 eV (784 nm), a bandwidth (FWHM) of 26 meV (13 nm), and an ellipticity of  $\approx 0.4$ . It is noteworthy that, in comparison with a perfectly circular polarization of the NIR, our numerical simulations reveal only a minor reduction of about 10 % in the expected CD. With a pulse duration of  $140 \text{ fs} \pm 30 \text{ fs}$  (FWHM), a focus spot size of  $150 \mu\text{m} \pm 50 \mu\text{m}$  (FWHM), and pulse energies ranging from  $30 \mu\text{J}$  to  $420 \mu\text{J}$ , laser intensities from  $0.9 \times 10^{12} \text{ W/cm}^2$  to  $1.1 \times 10^{13} \text{ W/cm}^2$  were available.

The helium gas was injected into the experimental chamber (background pressure  $\approx 6.5 \times 10^{-9} \text{ mbar}$ ) via supersonic expansion. In the center of a velocity map imaging (VMI) electron spectrometer<sup>25</sup>, the gas jet crossed the spatially overlapping, co-propagating XUV and NIR beams. The energy resolution of the VMI spectrometer was 90 meV (FWHM) at a kinetic energy of 0.1 eV and better than 200 meV over the entire range of the present investigation. Due to the applied setting of the VMI, electrons with kinetic energies of less than about 50 meV could not be reliably detected in our experiment, and hence their signal is not reported here.

### Theory

As indicated in the Introduction, we consider the case without an AC Stark shift in the preparation process of the ions. The XUV pulse first ionizes one of the  $1s$  electrons in the helium ground state and subsequently excites the other one to the  $3p$  level. After a delay of about 500 fs, which is very small compared to the lifetime of  $\approx 324 \text{ ps}$  of the  $\text{He}^+(3p)$  excited state<sup>28</sup>, the relaxation of the  $1s$  orbital from the neutral to the ionic configuration has taken place already, while no significant radiative decay of the excited ionic state has happened. We therefore solve the time-dependent Schrödinger equation (TDSE) for the active electron, which is the remaining bound electron after the initial ionization step of the  $\text{He}(1s^2)$  ground state<sup>17</sup>.

Consequently, we are dealing with a true one-electron target, whose nonrelativistic orbitals are known analytically<sup>29</sup>, while the continuum states on which to project the final-state wave function to obtain the ionization signal are pure Coulomb functions. Hence, we can start the calculation directly with a mixture of  $\text{He}^+$  ions in the  $1s$  ground state and the polarized  $\text{He}^+(3p, m=+1)$  state, from which the electron is removed by the co- or counter-rotating circularly polarized NIR field. For the parameters in the current experiment, the actual mixture of ions in the excited state and the ground state is irrelevant, since the NIR alone is too weak to seriously affect the  $1s$  electron.

Since reporting our earlier work<sup>17</sup>, we significantly enhanced the efficiency of the associated computer code through improved OpenMP parallelization and a variable radial grid in our finite-difference method<sup>30</sup>. Specifically, we take a smallest stepsize of 0.01 (we use atomic units in this section) near the nucleus and a largest stepsize of 0.05 for large distances. All these improvements made it possible to apply pulses of duration and peak intensity much closer to those used in the experiment, which could not be done previously<sup>17</sup>.

The calculations were carried out in the velocity gauge of the electric dipole operator. It is well known<sup>31,32</sup> that partial-wave convergence for long wavelengths is much faster in this gauge than in the length gauge. This aspect is crucial for the present problem, since we cannot use the simplifying cylindrical symmetry of linearly polarized light. Specifically, partial waves up to angular momenta  $\ell = 40$  were included in order to ensure converged results. Tests carried out by varying the time step, the radial grid, and the number of partial waves, as well as their magnetic quantum numbers, give us confidence in the numerical accuracy of the predictions. Most likely, the largest uncertainty originates from the fact that we make idealized assumptions about the experimental pulse, such as its length, shape, peak intensity, polarization, and carrier envelope phase, i.e., parameters that are generally difficult to determine accurately in the experiment.

In the present calculations, we took a 160-cycle pulse of the NIR laser (60 fs FWHM in intensity) with a sine-square envelope of the vector potential  $\mathbf{A}(t)$ , from which we calculated the electric field as  $\mathbf{E}(t) = -\partial \mathbf{A}(t)/\partial t$ . Setting the vector potential rather than the electric field directly avoids a possibly unphysical pulse with nonvanishing displacement<sup>33</sup>, although for long pulses like those employed here the effect of differentiating the envelope function is small. Furthermore, changing the carrier-envelope phase is not important for such pulses either. Finally, the target

created by the XUV pulse is very small compared to the spot irradiated by the NIR pulse. Hence, focal-point averaging of the NIR intensity over the interaction volume is not necessary either.

## Results and Discussion

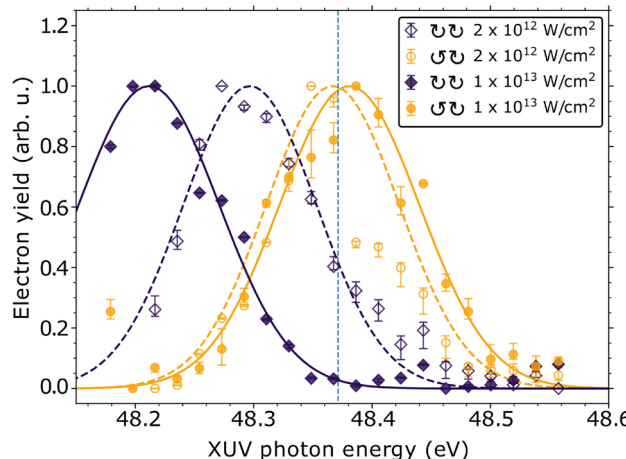
In order to validate the approach of using temporally separated XUV and NIR pulses to eliminate the influence of the NIR-induced AC-Stark shift on the population of the  $3p$  resonance in  $\text{He}^+$ , we first reproduced the conditions of the earlier experiment<sup>17</sup> performed with temporally overlapping pulses. Under these conditions the observed intensity-dependent changes of the CD are mainly caused by the polarization-dependent AC-Stark shift of the  $3p$  resonance<sup>34</sup>. To further test this interpretation, electron spectra were recorded while scanning the XUV pulses around the  $\text{He}^+(3p)$  resonance by varying the photon energy from 48.15 eV to 48.60 eV in the presence of the temporally overlapping optical laser.

The yields of the MPI and ATI photoelectrons, produced upon multiphoton ionization of the  $3p$  resonance by the NIR laser, are displayed in Fig. 2 as a function of the FEL photon energy for two NIR peak intensities with co- and counter-rotating circular laser polarization, respectively. As demonstrated by the experimental data and discussed in detail by Grum-Grzhimailo *et al.*<sup>34</sup>, the shift of the resonance position indeed strongly depends on both the relative helicity and the laser intensity. While for counter-rotating polarization the position coincides within the experimental resolution with the field-free position at 48.37 eV, the data recorded for co-rotating polarization clearly show a shift of the resonance, which grows with increasing NIR-laser intensities. The measured energy shifts of the resonance are 76 meV and 160 meV towards lower excitation energies for laser intensities of  $2 \times 10^{12} \text{ W/cm}^2$  and  $1 \times 10^{13} \text{ W/cm}^2$ , respectively. At  $2 \times 10^{12} \text{ W/cm}^2$ , the theoretical value is 90 meV. For the counter-rotating case, a shift towards higher energies of no more than 10 meV up to a laser intensity of  $6 \times 10^{12} \text{ W/cm}^2$  was calculated. Hence, if the pulses overlap as in our earlier work<sup>17</sup>, the observed dichroism is indeed strongly affected by how many ions are actually prepared in the oriented excited state under investigation. The population of this excited state, therefore, is one of the crucial parameters in determining the CD.

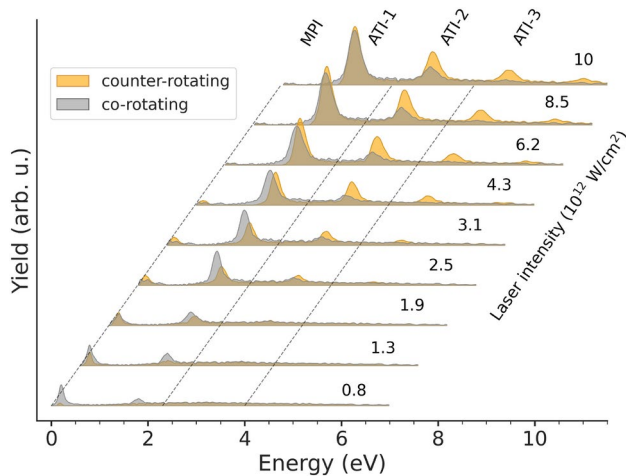
In order to eliminate the effect of this AC-Stark-shift-induced “preparation asymmetry” of the oriented ions, all further experiments were performed with the NIR pulses delayed by about 500 fs relative to the XUV. This makes it possible to analyze in detail the influence of the intense optical laser field on the ionization probabilities for different combinations of the circularly polarized XUV and NIR pulses, thus giving access to studying the Freeman resonances in better detail.

Figure 3 exhibits photoelectron spectra for a range of peak intensities of the optical laser for co- and counter-rotating circularly polarized pulses. We see strong intensity variations in the peak at the lowest kinetic energies (around 0.2 eV). At low intensities, the signal for co-rotating pulses stays nearly constant, while the signal is strongly increasing for counter-rotating pulses. As predicted in<sup>34</sup>, the MPI peak, which originates from the absorption of four NIR photons, quickly moves below threshold. The signal in the counter-rotating case remains almost constant up to an intensity of about  $4.3 \times 10^{12} \text{ W/cm}^2$ . This behavior results in the general trend of the CD observed earlier, i.e., a maximum circular dichroism of  $\approx +1$  at low NIR intensity, followed by a successive drop with increasing intensity (see Fig. 4). Figure 3 also clearly shows the first ATI peak (labeled ATI-1) at all displayed intensities, followed by the second (ATI-2) starting to be visible around  $2 \times 10^{12} \text{ W/cm}^2$ , and even a third (ATI-3) at the highest peak intensities.

As seen in Fig. 4, both experiment and theory predict nearly maximum values of the CD for the MPI line at the lowest peak intensity. However, the sign change of the CD, observed and discussed in the earlier experiments<sup>17</sup>, cannot be confirmed in the present study, where the influence of the AC-Stark shift to the population of the  $3p$



**Fig. 2.** Photoelectron yield generated by co- or counter-rotating polarized optical pulses depending on the XUV photon energy at NIR-laser intensities of  $2 \times 10^{12} \text{ W/cm}^2$  and  $1 \times 10^{13} \text{ W/cm}^2$ . The dashed vertical line marks the position of the  $3p$  resonance in the absence of the optical laser. The peaks for the co-rotating cases are shifted significantly to the left of the field-free line. Gaussian profiles (lines) were fitted to the experimental data points to highlight the polarization- and intensity-dependent shifts.



**Fig. 3.** Photoelectron spectra for different peak intensities of the optical laser for co- (darker shade) and counter-rotating (lighter shade) polarized NIR laser pulses. The zero lines for each peak intensity (indicated in multiples of  $10^{12} \text{ W/cm}^2$  on the right) have been offset to make the individual results visible.

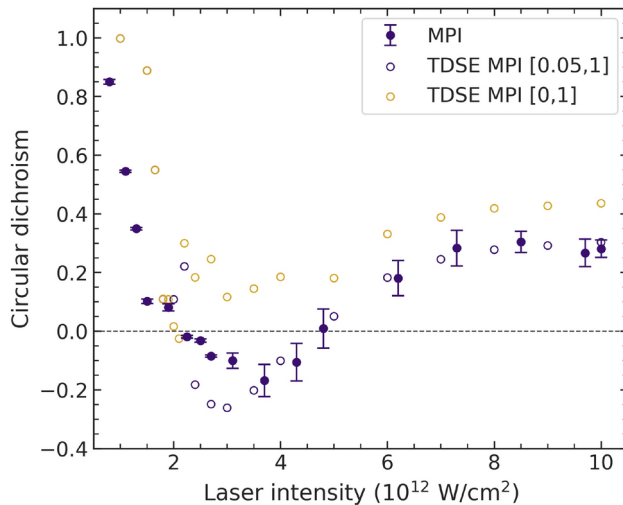


**Fig. 4.** Experimental and theoretical CD values at different NIR-laser peak intensities for the MPI feature of the photoelectron spectrum. The solid symbols with error bars represent the experimental data, while the TDSE predictions are shown as open symbols. The theoretical predictions are displayed once as adapted to the experimental conditions (blue) and again including all features down to zero kinetic energy (ocher). The numbers in parentheses of the legend indicate the kinetic energy range (in eV) that was accounted for in the integration over the theoretical MPI peak.

resonance in the ion was eliminated. Taking the experimental conditions into account also for the theory by cutting off the signal below 50 meV, a sign change around  $2 \times 10^{12} \text{ W/cm}^2$  and another sign change back to positive values around  $5 \times 10^{12} \text{ W/cm}^2$  are consistently found in both experiment and theory. The remaining differences predominantly originate from the experimental intensity uncertainty. However, the kinetic energy range from 0 to 50 meV is calculated to yield significant contributions to the CD of the MPI (ocher circles in Fig. 4). Theory thus predicts the CD of the MPI peak to stay positive throughout the intensity range of the present study.

We emphasize that in the current setup with non-overlapping pulses, the CD value is *not* affected by the presence of less ions in the initial state due to the NIR acting already during the preparation stage. Consequently, the AC-Stark shift, which was predicted to lead to negative CD values for the MPI, is strongly influencing the CD, but it is not the only process resulting in significant CD variations at low NIR intensities. Other phenomena have to be taken into account to explain the observations under the present conditions.

The general trend of the decreasing CD and the sign change for the MPI line can be explained by the complex interplay between the shift of the MPI line and channel closing, which is different in the co- and counter-rotating cases. While direct ionization by a four-photon process is no longer possible for intensities higher

than  $2.5 \times 10^{12} \text{ W/cm}^2$  in the case of co-rotating pulses, channel closing appears only at  $4.8 \times 10^{12} \text{ W/cm}^2$  for counter-rotating pulses, as calculated in<sup>34</sup>.

A simplified general structure of the energy levels in  $\text{He}^+$  in the presence of an intense external field is illustrated for the current situation in Fig. 5, i.e., after preparing the excited  $\text{He}^+(3p)$  state with right-handed circularly polarized XUV radiation. The peak position of the  $3p$  resonance hardly changes with increasing NIR intensity for the counter-rotating case, whereas it is shifted significantly towards lower excitation energies for the co-rotating case. This strong variation of the  $3p$  resonance position has, together with the general shift of the ionization threshold and the high-lying Rydberg states, also an effect on the MPI step. In the low-intensity regime, ionization of the  $3p$  resonance can be achieved by a four-photon process resulting in the ejection of electrons with kinetic energies of about 0.2 eV<sup>17</sup>. For increasing NIR intensities, the shift of the levels is transformed to a shift in the kinetic energy of the MPI electron, which rapidly moves towards (and ultimately below) the ionization threshold.

This behavior is very different from other observations of the circular dichroism in the ionization of polarized intermediate states. A multi-photon ionization study of the  $2p$  ( $m = +1$ ) state in atomic Li<sup>35</sup>, performed in the intensity regime  $0.3 - 1.3 \times 10^{12} \text{ W/cm}^2$ , does not show an intensity dependence of the CD, but instead a strong wavelength dependence. Furthermore, at higher intensities around  $8.5 \times 10^{14} \text{ W/cm}^2$ , where tunnel ionization is the dominating mechanism, ionization of Ar atoms with co-rotating pulses was found to be less likely than with counter-rotating pulses<sup>4</sup>. In the present investigation with external fields in the order of a few  $10^{12} \text{ W/cm}^2$ , the dynamics are much more complex, and the CD is determined by the interplay of different mechanisms.

Additional insight can be gained by analyzing the individual electron spectra created by multiphoton ionization at different intensities. Figures 6 and 7 show these spectra for the counter- and co-rotating cases, respectively, together with a few lineouts for selected intensities. The shift of the lines with increasing intensity is nicely seen in the ATI peaks. For the MPI line, which is presented on an enlarged scale in Figs. 6b and 7b, some internal structures besides the shift to lower kinetic energies are also visible and highlighted in the lineouts. For the counter-rotating case (cf. Fig. 6), a resonance is clearly seen around  $1.5 \times 10^{12} \text{ W/cm}^2$ . These features originate from Freeman resonances<sup>36</sup>, which at particular intensities become resonant for three-photon excitation of the  $3p$  state in the four-photon ionization process. Given the strength of the effect under the present conditions, we rule out substantial contributions due to energy shifts induced by nondipole effects, which were recently reported for strong-field and above-threshold ionization<sup>37,38</sup>. In the present case, these resonances are associated with  $6d$  ( $m = -2$ ) and  $6g$  ( $m = -2$ ), which are clearly separated energetically in theory<sup>34</sup>. However, they are only visible as a shift in the experimental spectra due to the finite energy resolution of the spectrometer.

For the co-rotating case (cf. Fig. 7), the appearance of the Freeman resonances is even more pronounced, and resonances with symmetry  $6g$  ( $m = +4$ ) and  $4f$  ( $m = +3$ ) can be identified around  $1.1 \times 10^{12} \text{ W/cm}^2$  and  $2.5 \times 10^{12} \text{ W/cm}^2$ . The qualitative agreement between experiment and theory is good, with some remaining differences in the details. Interestingly, we note substructures in the theoretical predictions for some, but not all, of the intensities. These interference structures are particularly pronounced for the  $6g$  ( $m = +4$ ) resonance in Fig. 7d, but are not resolved in the experiment. They arise from interfering wavepackets with the same kinetic energy, but formed at the leading and trailing edges of the pulse<sup>39</sup>. Finally, the persistent signal of the  $4f$  ( $m = +3$ ) resonance in the co-rotating case at high NIR intensities is the main reason for re-establishing positive CD values in the MPI line (cf. Fig. 4).

Generally, the influence of the Freeman resonances should also be visible in the high-energy ATI peaks, but the energy resolution of the experiment is limiting its observation. Besides a strong variation of their intensity

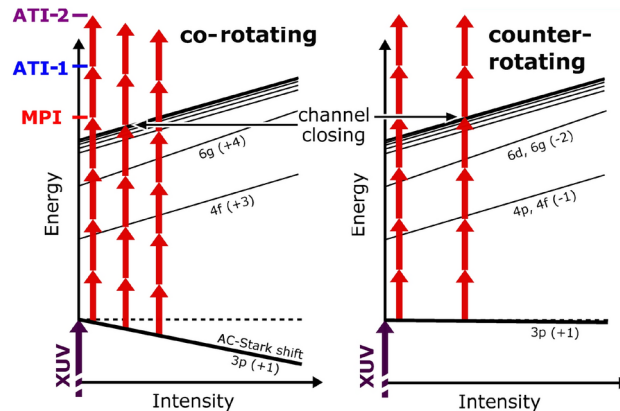


**Fig. 5.** Schematic illustration of multiphoton ionization from the  $\text{He}^+(3p)$  level for co- and counter-rotating polarized XUV and NIR pulses. The arrows represent the NIR and XUV photons, respectively. The tilted lines indicate various states. For a detailed discussion of the individual shifts and the most important intermediate resonance states involved, see<sup>34</sup>. Note that the four-photon channel, which leads to the main photoline (MPI), closes at significantly lower NIR intensity for the co-rotating (about  $2.5 \times 10^{12} \text{ W/cm}^2$ ) compared to the counter-rotating case (about  $4.8 \times 10^{12} \text{ W/cm}^2$ ). Also indicated are the first two above-threshold ionization lines ATI-1 and ATI-2.

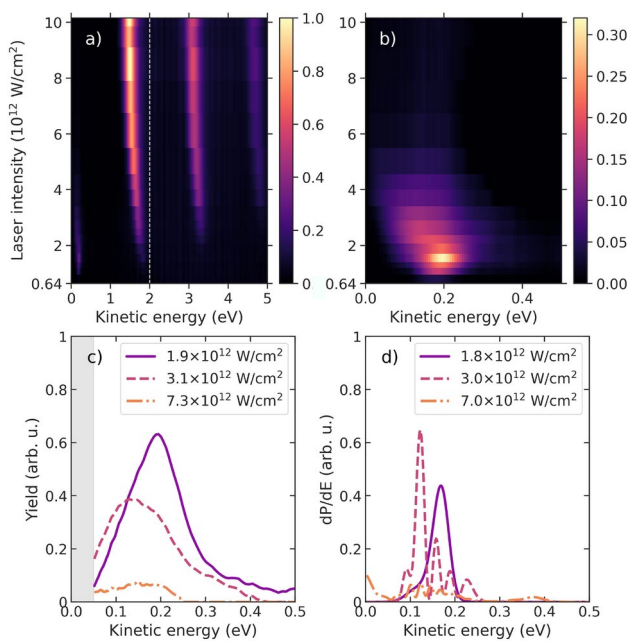


**Fig. 6.** Measured intensity dependence of the photoelectron spectrum for the counter-rotating case (a) for all features and (b) focused on the low-energy MPI feature. Note the different scales in the color bars to make the low-energy resonance visible. Panel (c) shows the experimental data as lineouts for the intensities indicated in the legend, with the corresponding theoretical results exhibited in panel (d). The gray-shaded area in (c) indicates the region in the experimental data affected by a lack of transmission and is thus neglected for the CD determination.

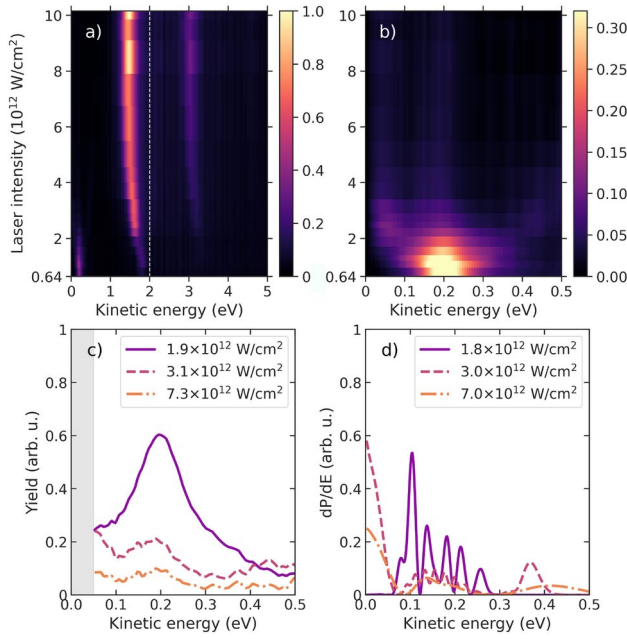


**Fig. 7.** Same as Fig. 6 for the co-rotating case.

ratios, the corresponding lines exhibit an intensity-dependent shift of their line positions, which is different for co- and counter-rotating pulses. The largest difference for ATI-1 is observed at  $3.1 \times 10^{12} \text{ W/cm}^2$  and amounts to 0.11 eV. For ATI-2 the most pronounced difference is found for the same intensity and amounts to 0.15 eV. This behavior is also visible in the numerical simulations and can be interpreted as another manifestation of the excitation of Freeman resonances in the multi-photon ionization pathway. Figure 8 shows an illustration of

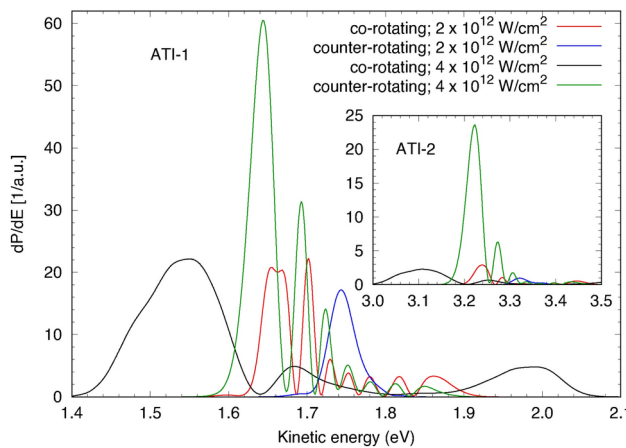


**Fig. 8.** Predicted ATI-1 and ATI-2 (inset) spectra for the co- and counter-rotating cases at IR peak intensities of  $2 \times 10^{12} \text{ W/cm}^2$  and  $4 \times 10^{12} \text{ W/cm}^2$ , respectively.

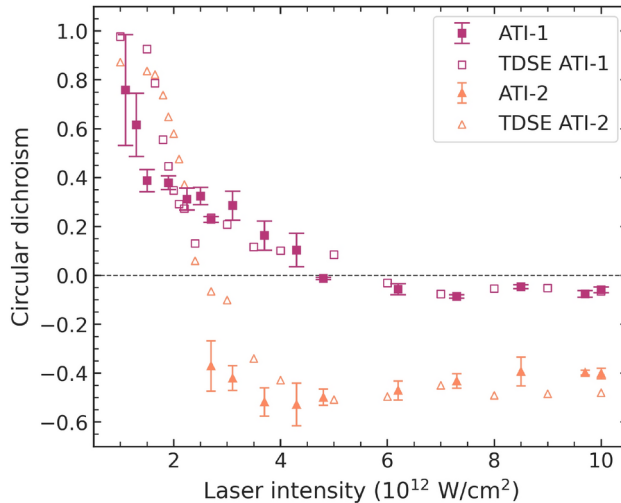


**Fig. 9.** Experimental and theoretical CD values at different laser peak intensities for the ATI-1 and ATI-2 features of the photoelectron spectrum. The solid symbols with error bars represent the experimental data, while the TDSE predictions are displayed as open symbols.

the complexity in the predicted spectra, which would require a much higher energy resolution to be validated experimentally.

The corresponding values for the circular dichroism of the ATI-1 and ATI-2 lines are shown in Fig. 9. The qualitative agreement between experiment (solid symbols) and theory (open symbols) is good. The remaining differences are most likely due to the uncertainties associated with the idealized representation of the theoretical pulses while there remain significant uncertainties in the experimental ones, in particular regarding the focus sizes and thus the absolute intensities. For the ATI-1 feature, the behavior of the CD is similar to the MPI feature, as it decreases from a value of  $\approx 1.0$  to slightly negative values at NIR-laser intensities exceeding  $6 \times 10^{12} \text{ W/cm}^2$ . Interestingly, the CD of the ATI-1 feature forms a plateau in the range  $2 - 3.5 \times 10^{12} \text{ W/cm}^2$ . This may be due to resonant transitions via high-lying Rydberg states, as channel closing appears at lower laser intensities for the co-rotating case. The theoretically predicted sharp drop of the CD at  $\approx 2.5 \times 10^{12} \text{ W/cm}^2$  is not resolved experimentally. At higher laser intensities, the CD decreases again towards zero when channel closing also occurs in the counter-rotating case.

While the present experiment cannot provide data in the low intensity region for ATI-2 due to a lack of signal (see Fig. 3), theory predicts a steep drop of the CD starting again near 1.0 and crossing zero around  $2.5 \times 10^{12} \text{ W/cm}^2$ . In this case, the drop in the CD continues towards large negative CD values that appear to approach  $\approx -0.5$  at high IR intensities. The experimental data are in good agreement with the predicted strongly negative CD in the ATI-2 peak. The lack of agreement for the low intensities may again be explained by the uncertainty in the absolute value of the experimental intensity as well as the statistical uncertainty of the data.

At the present time, we do not have an explanation for the trends observed in both experiment and theory for the distinctly different CDs in the MPI, ATI-1, and ATI-2 peaks. However, we hope that further studies on

the angular distributions associated with these peaks (currently ongoing in our laboratory) will reveal additional information regarding the dominant partial-wave contributions. Such results, together with propensity rules, may shed additional light on this issue.

## Conclusions and Outlook

We obtained the CD in the photoionization of oriented helium ions, specifically  $\text{He}^+(3p, m = +1)$ , for a variety of NIR intensities, independent of the oriented-state population. This allowed us to isolate dichroic effects and resonances and to map their intensity dependence not only for the main photoelectron line but also for the first and second ATI peaks. The circular dichroism of the main line assumes the maximum possible value of +1 at very low laser intensities. Due to the rapid channel closing for the co-rotating case, the CD of the MPI peak drops to small positive values before rising again at even higher intensities when the four-photon channel is nearly closed for both the co- and the counter-rotating cases and only the wings of the lines contribute to the ionization signal.

The CD for the ATI-1 and ATI-2 lines, which require a minimum of 5 and 6 photons, respectively, is also positive at the lowest intensities for which we obtained sufficiently strong signals. The CD for the ATI-1 line then decreases monotonically to slightly negative values with increasing NIR peak intensity, forming a small plateau between  $2 - 3 \times 10^{12} \text{ W/cm}^2$ , while the CD for the ATI-2 line drops from about +1 to strongly negative values around -0.5 at NIR peak intensities above  $3 \times 10^{12} \text{ W/cm}^2$ .

Even though the system under investigation represents a purely Coulombic one-electron problem, there are still many interesting features to be noticed, including substructures in the various peaks at particular intensities and the general trends seen in the CD for those peaks as a function of the NIR intensity. While the overall agreement between experiment and theory can be considered very satisfactory, with all principal features seen in both, simple models to explain many of these features are still missing.

A next step for shedding light on the missing links, e.g., to the studies of atomic Li, is to vary the IR wavelength in order to further investigate the effect of the various resonances and to distinguish their role from other fundamental effects. Furthermore, angle-resolved measurements should provide additional information about the dominant angular-momentum channels and the partial-wave composition of the various pathways involved.

## Data availability

The datasets used and analysed during the current study are available from the corresponding author upon reasonable request.

Received: 5 August 2024; Accepted: 4 October 2024

Published online: 08 November 2024

## References

1. Baier, S., Grum-Grzhimailo, A. & Kabachnik, N. Angular distribution of photoelectrons in resonant photoionization of polarized atoms. *J. Phys. B At. Mol. Opt. Phys.* **27**, 3363. <https://doi.org/10.1088/0953-4075/34/11/101> (1994).
2. Aloise, S., O'Keeffe, P., Cubaynes, D., Meyer, M. & Grum-Grzhimailo, A. Photoionization of synchrotron-radiation-excited atoms: Separating partial cross sections by full polarization control. *Phys. Rev. Lett.* **94**, 223002. <https://doi.org/10.1103/PhysRevLett.94.23002> (2005).
3. Logé, C. & Boesl, U. Multiphoton ionization and circular dichroism: new experimental approach and application to natural products. *Chem.Phys.Chem.* **12**, 1940. <https://doi.org/10.1002/cphc.201100035> (2011).
4. Eckart, S. et al. Ultrafast preparation and detection of ring currents in single atoms. *Nat. Phys.* **14**, 701. <https://doi.org/10.1038/s41567-018-0080-5> (2018).
5. De Silva, A. et al. Using circular dichroism to control energy transfer in multiphoton ionization. *Phys. Rev. Lett.* **126**, 023201. <https://doi.org/10.1103/PhysRevLett.126.023201> (2021).
6. Gryzlova, E. et al. Isotope effects in resonant two-color photoionization of Xe in the region of the  $5p^5(2P_{1/2})4f[5/2]_2$  autoionizing state. *New J. Phys.* **17**, 043054. <https://doi.org/10.1088/1367-2630/17/4/043054/meta> (2015).
7. Ritchie, B. Theory of the angular distribution for ejection of photoelectrons from optically active molecules and molecular negative ions, II. *Phys. Rev. A* **14**, 359. <https://doi.org/10.1103/PhysRevA.14.359> (1976).
8. Böwering, N. et al. Asymmetry in photoelectron emission from chiral molecules induced by circularly polarized light. *Phys. Rev. Lett.* **86**, 1187. <https://doi.org/10.1103/PhysRevLett.86.1187> (2001).
9. Nahon, L., Garcia, G. A. & Powis, I. Valence shell one-photon photoelectron circular dichroism in chiral systems. *J. Electron Spectrosc. Relat. Phenomena* **204**, 322 (2015).
10. Beaulieu, S. et al. Photoexcitation circular dichroism in chiral molecules. *Nat. Phys.* **14**, 484 (2018).
11. Ilchen, M. et al. Site-specific interrogation of an ionic chiral fragment during photolysis using an X-ray free-electron laser. *Commun. Chem.* **4**, 119 (2021).
12. Veyrinas, K. et al. Dissociative photoionization of  $\text{NO}$  across a shape resonance in the XUV range using circularly polarized synchrotron radiation. *J. Chem. Phys.* **151**, 174305 (2019).
13. van der Laan, G. & Figueroa, A. I. X-ray magnetic circular dichroism—a versatile tool to study magnetism. *Coord. Chem. Rev.* **277**, 95 (2014).
14. Barth, I. & Smirnova, O. Nonadiabatic tunneling in circularly polarized laser fields: Physical picture and calculations. *Phys. Rev. A* **84**, 063415. <https://doi.org/10.1103/PhysRevA.84.063415> (2011).
15. Mazza, T. et al. Determining the polarization state of an extreme ultraviolet free-electron laser beam using atomic circular dichroism. *Nat. Commun.* **5**, 1. <https://doi.org/10.1038/ncomms4648> (2014).
16. Kazansky, A., Grigorieva, A. & Kabachnik, N. Circular dichroism in laser-assisted short-pulse photoionization. *Phys. Rev. Lett.* **107**, 253002. <https://doi.org/10.1103/PhysRevLett.107.253002> (2011).
17. Ilchen, M. et al. Circular dichroism in multiphoton ionization of resonantly excited  $\text{He}^+$  ions. *Phys. Rev. Lett.* **118**, 013002. <https://doi.org/10.1103/PhysRevLett.118.013002> (2017).
18. Hartmann, G. et al. Circular dichroism measurements at an X-ray free-electron laser with polarization control. *Rev. Sci. Instrum.* **87**, 083113 (2016).
19. Mazza, T. et al. Angular distribution and circular dichroism in the two-colour XUV + NIR above-threshold ionization of helium. *J. Mod. Opt.* **63**, 367. <https://doi.org/10.1080/09500340.2015.1119897> (2016).

20. Rörig, A. et al. Multiple-core-hole resonance spectroscopy with ultraintense X-ray pulses. *Nat. Commun.* **14**, 5738 (2023).
21. Freeman, R. & Bucksbaum, P. Investigations of above-threshold ionization using subpicosecond laser pulses. *J. Phys. B: At. Mol. Opt. Phys.* **24**, 325. <https://doi.org/10.1088/0953-4075/24/2/004> (1991).
22. Marchenko, T., Muller, H., Schafer, K. & Vrakking, M. Wavelength dependence of photoelectron spectra in above-threshold ionization. *J. Phys. B: At. Mol. Opt. Phys.* **43**, 185001. <https://doi.org/10.1088/0953-4075/43/18/185001> (2010).
23. Allaria, E. et al. Control of the polarization of a vacuum-ultraviolet, high-gain, free-electron laser. *Phys. Rev. X* **4**, 041040. <https://doi.org/10.1103/PhysRevX.4.041040> (2014).
24. Bauer, J. H., Mota-Furtado, F., O'Mahony, P. F., Piraux, B. & Warda, K. Ionization and excitation of the excited hydrogen atom in strong circularly polarized laser fields. *Phys. Rev. A* **90**, 063402. <https://doi.org/10.1103/PhysRevA.90.063402> (2014).
25. Lyamayev, V. et al. A modular end-station for atomic, molecular, and cluster science at the Low-Density-Matter beamline of FERMI@Elettra. *J. Phys. B: At. Mol. Opt. Phys.* **46**, 164007. <https://doi.org/10.1088/0953-4075/46/16/164007> (2013).
26. Allaria, E. et al. Highly coherent and stable pulses from the fermi seeded free-electron laser in the extreme ultraviolet. *Nat. Photonics* **6**, 699. <https://doi.org/10.1038/nphoton.2012.233> (2012).
27. Kramida, A. E., Ralchenko, Y. & Reader, and NIST ASD Team, NIST Atomic Spectra Database, (version 5.10). <https://www.nist.gov/pml/atomic-spectra-database> (2022).
28. Baumann, M. & Eibofner, A. Lifetime of the 3p state of ionized helium. *Phys. Lett. A* **35**, 173. [https://doi.org/10.1016/0375-9601\(71\)90132-0](https://doi.org/10.1016/0375-9601(71)90132-0) (1971).
29. Bethe, H. & Salpeter, E. *Quantum Mechanics of One- and Two-Electron Atoms* (Springer, 2013). <https://books.google.de/books?id=nxz2CAAAQBAJ>.
30. Douguet, N., Guchkov, M., Bartschat, K. & Santos, S. F. d. Efficient time-dependent method for strong-field ionization of atoms with smoothly varying radial steps. *Atoms* **12**, 89. <https://doi.org/10.3390/atoms12070034> (2024).
31. Cormier, E. & Lambropoulos, P. Optimal gauge and gauge invariance in non-perturbative time-dependent calculation of above-threshold ionization. *J. Phys. B: At. Mol. Opt. Phys.* **29**, 1667. <https://doi.org/10.1088/0953-4075/29/9/013> (1996).
32. Grum-Grzhimailo, A. N., Abeln, B., Bartschat, K., Weflen, D. & Urness, T. Ionization of atomic hydrogen in strong infrared laser fields. *Phys. Rev. A* **81**, 043408. <https://doi.org/10.1103/PhysRevA.81.043408> (2010).
33. Ivanov, I. A. et al. Displacement effect in strong-field atomic ionization by an XUV pulse. *Phys. Rev. A* **90**, 043401. <https://doi.org/10.1103/PhysRevA.90.043401> (2014).
34. Grum-Grzhimailo, A. N., Douguet, N., Meyer, M. & Bartschat, K. Two-color XUV plus near-IR multiphoton near-threshold ionization of the helium ion by circularly polarized light in the vicinity of the 3p resonance. *Phys. Rev. A* **100**, 033404. <https://doi.org/10.1103/PhysRevA.100.033404> (2019).
35. De Silva, A. H. N. C. et al. Circular dichroism in atomic resonance-enhanced few-photon ionization. *Phys. Rev. A* **103**, 053125. <https://doi.org/10.1103/PhysRevA.103.053125> (2021).
36. Freeman, R. R. et al. Above-threshold ionization with subpicosecond laser pulses. *Phys. Rev. Lett.* **59**, 1092. <https://doi.org/10.1103/PhysRevLett.59.1092> (1987).
37. Hartung, A. et al. Electric nondipole effect in strong-field ionization. *Phys. Rev. Lett.* **126**, 053202. <https://doi.org/10.1103/PhysRevLett.126.053202> (2021).
38. Lin, K. et al. Magnetic-field effect in high-order above-threshold ionization. *Phys. Rev. Lett.* **128**, 023201. <https://doi.org/10.1103/PhysRevLett.128.023201> (2022).
39. Wang, S., Jiang, W.-C., Tian, X.-Q. & Sun, H.-B. Conjoint influence of quantum interference and freeman resonance on substructures of the photoelectron spectra in above-threshold ionization. *Phys. Rev. A* **101**, 053417. <https://doi.org/10.1103/PhysRevA.101.053417> (2020).

## Acknowledgements

The authors are grateful for fruitful discussions with Thomas Pfeifer and Christian Ott from the Max Planck Institute for Nuclear Physics in Heidelberg, Germany. The authors furthermore acknowledge the invaluable support of the technical and scientific staff of FERMI at Elettra-Sincrotrone Trieste. R.W. and M.Me. acknowledge funding by the Deutsche Forschungsgemeinschaft (DFG) in SFB-925, “Light induced dynamics and control of correlated quantum systems”, project No. 170620586. M.I., V.M., and Ph.S. acknowledge funding for a Peter-Paul-Ewald Fellowship from the Volkswagen foundation. M.I. acknowledges support from the DFG under Project No. 328961117 in SFB-1319, “Extreme light for sensing and driving molecular chirality”. M.I., N.W., and M.Me. were supported by the DFG Cluster of Excellence “CUI: Advanced Imaging of Matter”, project No. 390715994. The theoretical part of this work was funded by the NSF under grant Nos. PHY-2110023 and PHY-2408484 (K.B.), No. PHY-2012078 (N.D.), and by the ACCESS supercomputer allocation No. PHY-090031. The work of Alexei N. Grum-Grzhimailo was performed before the start of the Ukrainian war.

## Author contributions

M.Me., M.I., A.G.G. and K.B. conceived the experiment. R.W., M.I., P.S., C.C., A.D., G.D.N., M.D.F., J.H., M.Ma., V.M., O.P., K.C.P., D.R., M.Z., and M.Me. performed the experiment. R.W., P.S., and N.W. analyzed the experimental data. N.D., Z.D., A.G.G., and K.B. performed all theoretical calculations. R.W., M.I., N.D., K.B., and M.Me. interpreted the results and wrote the manuscript. All authors contributed to the final version of the paper.

## Funding

Open Access funding enabled and organized by Projekt DEAL.

## Competing interests

The authors declare no competing interests.

## Additional information

**Correspondence** and requests for materials should be addressed to M.Me.

**Reprints and permissions information** is available at [www.nature.com/reprints](https://www.nature.com/reprints).

**Publisher's note** Springer Nature remains neutral with regard to jurisdictional claims in published maps and institutional affiliations.

**Open Access** This article is licensed under a Creative Commons Attribution 4.0 International License, which permits use, sharing, adaptation, distribution and reproduction in any medium or format, as long as you give appropriate credit to the original author(s) and the source, provide a link to the Creative Commons licence, and indicate if changes were made. The images or other third party material in this article are included in the article's Creative Commons licence, unless indicated otherwise in a credit line to the material. If material is not included in the article's Creative Commons licence and your intended use is not permitted by statutory regulation or exceeds the permitted use, you will need to obtain permission directly from the copyright holder. To view a copy of this licence, visit <http://creativecommons.org/licenses/by/4.0/>.

© The Author(s) 2024